Preprints, 10th IFAC International Symposium on
Advances in Automotive Control
Columbus, Ohio, USA, August 28-30, 2022

Extremum Seeking Control-based Control Framework for Electric Vehicle Platooning

Zifei Su* and Pingen Chen**

*Department of Mechanical Engineering, Tennessee Technological University, Cookeville, TN 38505 USA (*e-mail: zsu42@tntech.edu; **e-mail:pchen@tntech.edu)*

Abstract: Battery electric vehicles (BEVs) are more commonly deployed in short-distance and in-city operations than in long-distance on-highway operations mainly due to range anxiety. One of the solutions to alleviate the range anxiety is platooning. Vehicle platooning with short distances has demonstrated significant improvements in vehicle efficiency by reducing the aerodynamic drag force. To maximize the energy saving benefit brought by vehicle platooning, it is critical to identify the inter-vehicle space that results in the most reduction of aerodynamic drag coefficient in real time and appropriately maintain the inter-vehicle distance, which is a rather challenging task due to the unknown correlation between the inter-vehicle space and aerodynamic drag coefficient. This paper proposes a unified extremum seeking control (ESC)-based control framework to find and maintain the inter-vehicle distance that corresponds to the minimum air drag coefficient in presence of the environment uncertainty. The controller is implemented on a BEV model with a one-pedal driving (OPD) feature and validated in simulation. Simulation results demonstrated that the proposed ESC-based control framework can effectively identify the inter-vehicle distance with respect to the minimum aerodynamic drag coefficient in real time and regulate the inter-vehicle distance at the desired value without steady-state oscillations. The proposed framework can potentially be applied to both passenger BEVs and commercial BEVs to improve vehicle efficiency.

Keywords: Battery Electric Vehicle, One Pedal Driving, Extremum Seeking Control, Vehicle Platoon.

1. INTRODUCTION

For battery electric vehicles (BEVs) including passenger BEVs and commercial BEVs, range anxiety is one of the most important reasons that limits the acceptance and adoption. Although the driving range of BEVs has been significantly increased in the past decade due to the continuing development of battery technologies, range anxiety is still one major obstacle on the real-world application. Range anxiety can be mitigated with several strategies like optimization of the design and locations of charging stations, traffic assignment for electric vehicle (EV) network with limited charging infrastructure, and vehicle platoon. Platooning is relatively mature and more ecological than the other methods. A BEV with an adaptive cruise controller has the capability to follow a short inter-vehicle distance from leading vehicle on to reduce aerodynamic force.

The aerodynamic drag coefficient of the following vehicle in platooning varies with inter-vehicle distance. Simulation using Computational fluid dynamics (CFD) model shows that the air drag coefficient starts to drop at 5 body lengths as inter-vehicle distance decreases and reaches a minimum point at around 1.5 body lengths Davila et al (2013). In addition, the correlation between the inter-vehicle space and the drag coefficient may change with different vehicle types. To maximize the benefits of vehicle platoon, it is important to design a space controller to keep the inter-vehicle distance at where the air drag coefficient is minimum. However, according to the wind tunnel experiment report in Zabat et al (1995), the distance that corresponds to the minimum air drag coefficient may vary in different platooning scenarios. The complexity of drag coefficient model, in combination with the uncertainties from the lead vehicle (e.g., types and shapes) and the environment (e.g., wind speed) in real-world operation, make it difficult and expensive to test and quantify the optimal inter-vehicle distance for platooning by off-line measurements. Therefore, a real-time optimization method which can effectively and quickly identify the optimal inter-vehicle space for minimizing the aerodynamic force during platooning, is much needed.

Extremum seeking control (ESC) is a powerful algorithm which can seek the extrema of a certain cost function of a system in real time. An advantage of extremum seeking control is that the object function is not necessary to be known. once it has a local or global extrema. In this study, ESC is adopted to identify the optimal inter-vehicle space. To the author's knowledge, the applications of ESC on vehicle platoons have been rarely studied. However, the performance of a similar method aims for drag reduction on formation flights have been proved in Ryan (2012). Traditional ESC algorithm estimates the gradient of object function by perturbing its input with a periodic dither signal and by processing its output. After the object function reaches the extrema, the input will oscillate around the optimal value because of the periodic dither signal. In platoon, a periodic inter-vehicle distance is not preferred in that it has negative effect on driving comfort, safety and the energy consumption. Therefore, it is critical to address the steady-state oscillation issue when an extremum seeking control is applied.

The contribution of this paper is threefold: 1) An ESC-based control scheme is proposed to optimize the inter-vehicle space in platooning to achieve the minimum air drag coefficient; 2)

a robust sliding mode controller is implemented to track the generated optimal inter-vehicle distance and overcome potential system uncertainties; 3) an ESC without steady state oscillation (ESCWAO) is applied to address the steady-state oscillation issue which is encountered by the traditional ESC. The ESCWAO algorithm can help improve driving comfort while maximizing the platooning benefit. The proposed ESC-based controller is implemented and validated on a BEV model with a one pedal driving (OPD) feature in simulation.

The rest of the paper is organized as follows: Section 2 introduces the mathematic models. In Section 3, the ESC-based controller is described in details. Section 4 shows the simulation setup, results and analysis. Finally, concluding remarks and future work are discussed in Section 5.

2. TWO-VEHICLE PLATOON MODEL

2.1 Model of Vehicle Platoon

First, define x_1 and x_2 as the relative position and relative velocity between the leading and following vehicle, respectively, and the dynamics is described in (1) and (2).

$$\dot{x_1} = x_2 \tag{1}$$

$$\dot{x_2} = a_l - a_f \tag{2}$$

Then, according to road-load equation, the total driving force of the following vehicle, F_d, can be described in (3),

$$F_d = F_{acc} + F_{ad} + F_g + F_r \tag{3}$$

where $F_{acc} = m_f a_f$ is the vehicle acceleration force; $F_{ad} = \frac{1}{2} C_d(x_1) \rho A \left(v_f - v_w\right)^2$ is the aerodynamic drag resistance; $F_g = m_f g sin\left(\beta(t)\right)$ is the gradient resistance, $F_r = m_f C_r g cos\left(\beta(t)\right)_r$ is the rolling resistance. Among all the parameters of the expressions, m_f is the mass of the following vehicle; C_d is the air drag coefficient that changes with inter-vehicle distance; ρ is the air density; A is the frontal area of the vehicle, $v_w$is the wind speed, g is the acceleration of gravity, C_r is the rolling resistance coefficient and β is the road grade. In this paper, v_w and β are assumed to be constants.

According to the road-load equation, the dynamics of x_2 in (2) can be extended to (4).

$$\dot{x_2} = a_l - \frac{F_d}{m_f} + C_r g cos(\beta) + g sin(\beta) + \frac{\rho C_d(x_1) A v_f^2}{2 m_f} \tag{4}$$

For this system, F_d is assumed to be the system input, a_l and C_d are assumed to be unknown during vehicle platooning.

2.2 Energy Consumption Model

For the verification purpose, the overall energy consumption needs to be calculated. First, motor torque can be found in (5).

$$T_m = \frac{F_d r}{\xi_f} \tag{5}$$

Where T_m represents the motor torque, r represents the wheel radius and $\xi_f$is the final drive ratio. Similarly, the motor speed ω_m can be calculated by (6).

$$\omega_m = \frac{\xi_f v_f}{r} \tag{6}$$

Then, the motor power can be found in (7).

$$P_m = \begin{cases} \dfrac{T_m \omega_m}{\eta_m(T_m, \omega_m)} & T_m > 0 \\ 0 & T_m = 0 \\ T_m \omega_m \eta_m(T_m, \omega_m) & T_m < 0 \end{cases} \tag{7}$$

where η_m represents the motor efficiency. Finally, the energy consumption is obtained in (8).

$$E = \int_0^t P_m \, dt \tag{8}$$

2.3 Overall Model Structure

The proposed control algorithm is implemented on a simplified EV model with an OPD map. There are three regions in the OPD torque map including acceleration region, coasting region and braking region, based both on vehicle speed and angle of the pedal Boekel (2015). The two-dimensional torque map was built based on the data collected from field tests. Based on the OPD torque map, OPD power map can be generated as well which is also indexed by vehicle speed (v_f) and pedal percentage ($P\%$). Furthermore, an inverse OPD power map is generated to output pedal percentage based on driving power demand and vehicle speed. With the inverse OPD power map, the demand of driving power ($P_{d,c}$) from the proposed ESC can be converted into the pedal percentage demand. The pedal percentage demand in combination of vehicle speed can then decide actual driving power output ($P_{d,a}$) based on the OPD map. The flow of signals related to the OPD feature is illustrated in Fig. 1.

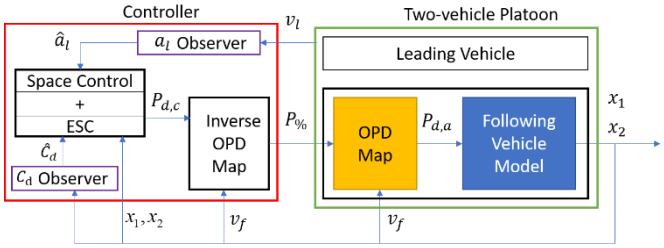

Fig. 1. The BEV with OPD Model and Control Framework

3. ESC-BASED CONTROL FRAMEWORK

The proposed control algorithm shown in Fig.1 contains four parts: 1) a high gain input observer to estimate the acceleration of leading vehicle; 2) a high gain observer to estimate air drag coefficient; 3) a robust sliding mode space controller to track the desired distance; 4) an extremum seeking controller without steady state oscillation to find the optimal desired distance. The details of each block can be provided in the following subsections.

3.1 High Gain Observer for C_d Estimation

C_d is critical to the extremum seeking, since it is not measurable, a high-gain input observer is designed for C_d estimation using the high-gain input observer technique

reported in Stotsky et al (2002). The accuracy of C_d estimation $\hat{C}_d$ is directly related to the performance of optimization.

Equation (4) can be rewritten in (13) to consider C_d as the input of the nonlinear system.

$$\dot{v_f} = f + hC_d \tag{13}$$

where

$$f = \frac{F_d}{m_f} - C_r g cos(\beta) - g sin(\beta) \tag{14}$$

$$h = -\frac{\rho A v_f^2}{2m_f} \tag{15}$$

Proposition 1: With the high-gain input observer designed in (16), the estimation error of C_d will be limited by a sufficient small value.

$$\hat{C}_d = \frac{\gamma v_f - \epsilon}{h} \tag{16}$$

where γ is an artificially selected positive design parameter and ε is a scalar variable whose dynamics is defined in (17).

$$\dot{\epsilon} = -\gamma\epsilon + \gamma f + \gamma^2 v_f \tag{17}$$

Proof: First, let the estimation error be in (18).

$$\nu = \gamma v_f - \epsilon - U \tag{18}$$

where $U = hC_d$. Then, select a Lyapunov function candidate in (19).

$$V_1 = \frac{\nu^2}{2} \tag{19}$$

Then, the time derivative of V_1 can be easily found and rearranged in (20) according to (17) and (18).

$$\dot{V}_1 = \nu[-\gamma\nu - \dot{U}] \tag{20}$$

SinceC_d, $\dot{C}_d$ v_f and a_f are physically bounded and take system uncertainty into consideration, it is reasonable to assume $\dot{U}$ is bounded by some constant $|\dot{U}|_{max}$. Then, the derivative of V_1 follows the inequality:

$$\dot{V}_1 \le -\gamma|v|^2 + |\dot{U}|_{max}|\nu| \tag{21}$$

The right-hand side of (21) can be re-organized as:

$$\dot{V}_1 \le -\gamma\left(|\gamma| - \frac{|\dot{U}|_{max}}{2\gamma}\right) + \frac{|\dot{U}|_{max}^2}{4\gamma} \tag{22}$$

Thus, $\dot{V}_1 \le 0$ when $|\nu| \ge \frac{|\dot{U}|_{max}}{\gamma}$. Therefore, by choosing a large γ, the estimation error ν can be sufficiently small. Then,$\widehat{U}$ can be designed in (23) based on (18) Chen (2014):

$$\widehat{U} = \gamma v_f - \epsilon \tag{23}$$

According to definition of U, $\hat{C}_d$ can be calculated in (30).

$$\hat{C}_d = \frac{\gamma v_f - \epsilon}{h} \tag{24}$$

Thus, the proposition is proved. Since input observer for a_l estimation using v_l measurement has the same design procedure, the observer design and proof will not be provided in this paper. The performance of the observer under dynamic conditions is proven in Yang et al (2021).

3.2 Spacing Controllers

The sliding mode controller designed in the author's previous work Yang et al (2021) is as a low-level space controller. The controller performance has been proved by both simulation and field tests. The control law is designed as:

$$F_d = m_f((F+\eta)\, sat(\frac{s}{\phi}) + \hat{f}_2 - \ddot{x}_{1,d} + \lambda\dot{\tilde{x}}_1) \tag{31}$$

where $\lambda > 0$ and $\eta > 0$ are the artificially designed parameters; $\tilde{x}_1 = x_1 - x_{1,d}$ is the error between the actual inter-vehicle distance and the desired distance; ϕ is the boundary layer thickness which can be selected artificially to avoid severe chattering issue; s is the sliding surface that defined as below.

$$s = \dot{\tilde{x}}_1 + \lambda\tilde{x}_1 \tag{32}$$

$\hat{f}_2$ represents the actual system dynamics h uncertainties included as shown in (33).

$$\hat{f}_2 = \frac{\hat{C}_d\rho A v_f^2}{2m_f} + C_r g cos\left(\hat{\beta}(t)\right) + g sin\left(\hat{\beta}(t)\right) + \hat{a}_l \tag{33}$$

where $\hat{C}_d$ is the estimated air drag coefficient by the input observer; $\hat{\beta}(t)$ represents the actual road grade; $\hat{a}_l$ is the estimated leading vehicle acceleration. Since all of the terms mentioned above are physically bounded, it is reasonable to assume the difference between the actual values and setup values are bounded. Then, define the upper boundary F that is denoted in (34).

$$F = \frac{\rho A v_f^2}{2m_f}|\tilde{C}_d|_{max} + C_r g\, cos\left(|\tilde{\beta}|_{max}\right) + g\, sin(|\tilde{\beta}|_{max}) + |\tilde{a}_l|_{max} \ge |\tilde{f}_2| \tag{34}$$

Then, select a Lyapunov Candidate function as shown in (35).

$$V_2 = \frac{1}{2}s^2 \tag{35}$$

The sliding reachability condition can be satisfied in (36):

$$\dot{V}_2 = \frac{1}{2}\frac{d}{dt}s^2 \le -\eta|s| \tag{36}$$

The details of the stability proof can be found in Yang (2021).

3.3 Extremum Seeking Controller

For extremum seeking controllers, a sinusoidal perturbation is added to the controller to allow the algorithm to locally optimize an objective function. Due to the nature periodical signal, oscillations are expected at steady states if a standard ESC is applied Wang et al (2016), Bhattacharjee et al (2021). This is undesirable in the platooning application as it will cause frequent acceleration and deceleration and thus deteriorate driving comfort and energy consumption. To address this issue, a novel ESC with attenuated steady-state oscillation (ESCWAO) reported in Bhattacharjee et al (2021)., was adopted in this study. The magnitude of the dither signal was

designed to attenuate with the decrease of estimated gradient. The structure of ESCWAO for a general single input and single output (SISO) nonlinear system is shown in Fig.2.

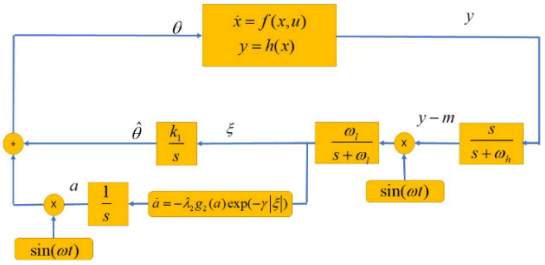

Fig. 2. Structure of ESCWAO Control Framework

According to the structure, the system dynamics can be described from (37) to (41).

$$\dot{x} = p\left(x, \alpha\left(x, \theta^* + \tilde{\theta} + asin(\omega t)\right)\right) \quad (37)$$

$$\dot{\tilde{\theta}} = k_1 \xi \quad (38)$$

$$\dot{\tilde{m}} = -\omega_h \tilde{m} + \omega_h\left(q(x) - q \circ l(\theta^*)\right) \quad (39)$$

$$\dot{\xi} = -\omega_l \xi + \omega_l (q(x) - q \circ l(\theta^*) - \tilde{m}) sin(\omega t) \quad (40)$$

$$\dot{a} = -\lambda_2 g_2(a) exp(-\gamma|\xi|) \quad (41)$$

In this case, $x = \left[x_1, x_2\right]^T$ and $p(x) = -100\hat{C}_d^2(x)$ which is the objective function. Although the $\hat{C}_d$ is available, the relationship between $\hat{C}_d$ and x_1 is unknown. $\tilde{\theta} = \hat{\theta} - \theta^*$ with θ^* as the optimal point; $\tilde{m} = m - q \circ l(\theta^*)$ with m as the low frequency components in y; ω, ω_l, ω_h, k_1, λ_2, γ, $\hat{\theta}(0)$ and $a(0)$ are the tuning parameters. The proof of convergence of ESCWAO is similar to the standard ESC despite the discussion about the attenuating magnitude of dither signal. Since it is well discussed in Bhattacharjee et al (2021), only the simple prerequisites for the convergence of standard ESC will be checked, Ariyur and Krstić (2003).

1. There exists a smooth function $l: R \to R^n$, such that the system with control law $u = \alpha(x, \theta)$, denoted as $\dot{x} = p\left(x, \alpha(x, \theta)\right) = 0$ if and only if $x = l(\theta)$. It indicates that the equilibrium point must be parametrized by θ. In this case, θ is x_d, $l(x_d) = x_d$ which satisfies Assumption 1.

2. For each $\theta \in R$, the equilibrium point,$x = l(\theta)$, is locally exponentially stable. According to the proof of the Lyapunov-based space controller in previous section, Assumption 2 is thus satisfied.

3. There exist $\theta^* \in R$ such that the following two conditions are satisfied.

$$(q \circ l)'(\theta^*) = 0$$

$$(q \circ l)''(\theta^*) < 0$$

Finally, with the results shown in Davila (2013), the Assumption 3 holds. The stability of standard extremum seeking control can be proved with the above three assumptions satisfied.

4. SIMULATION RESULTS AND DISCUSSION

4.1 Simulation Setup

The model used in the simulation is a simplified model based on the high-fidelity model proposed by Schafer and Chen (2020). The vehicle is equipped with a "e-Pedal" mode (i.e., OPD) and a 40-kWh battery and an electric motor with maximum power up to 120 kW. The motor efficiency map is from a high-fidelity 2013 Nissan Leaf model in Autonomie. The Nissan Leaf EV is rated with 239.79-km range, according to EPA. The performance of the proposed control framework on the BEVs' driving range is investigated by comparing the trip length with a 50% change of state of charge (SOC). The leading vehicle speed profile is obtained by repeating the speed profile in Fig. 3.

For comparison purposes, the standard ESC was also applied. The difference between the standard ESC and ESCWAO is the steady-state oscillation. To demonstrate the advantage of ESC over non-ESC method on optimizing the inter-vehicle distance, a baseline inter-vehicle space control was also generated and implemented with a predefined inter-vehicle space reference (x_d = 15 m). The abovementioned three controllers are denoted as "ESCWAO", "StandardESC", and "Baseline", respectively. The initial inter-vehicle distance is 30 m. $v_f(0) = 17$m/s. The road gradeβ is assumed to be 0.ρ =1.28 kg/m^3 and $g = 9.81m/s^2$. The main parameters for the following vehicle are designed as $C_r = 0.01$, $A = 2.5334m^2$, and $m_f = 1618.87kg$. The parameters for the sliding mode controller are selected as $\eta = 0.1, \lambda = 1$, and $\phi = 0.15$. The tunable parameters related to ESCWAO are parameters are designed as: $\omega_h = 4$, $\omega_l = 0.5$, $\omega = 1$, $k = 0.675$, $\hat{x}_d(0) = 15.45$, $a(0) = 5$, $\lambda_2 = 0.5$, and $\gamma = 5$. The parameters of standard ESC are tuned as: $\omega_h = 4$, $\omega_l = 0.5$,$\hat{\theta}(0) = \hat{x}_d(0) = 16$, the amplitude of perturbation signal for x_d to swing is selected as $a_1 = 0.3$, the other one for the gradient is selected as $a_2 = 1$. Although the initial relative distance is 30m, which seems to result in a flat region for C_d, the controller will still work since the ESC is applied to the desired relative distance and the choices of initial values will provide enough gradient information.

4.2 Simulation Results and Discussion

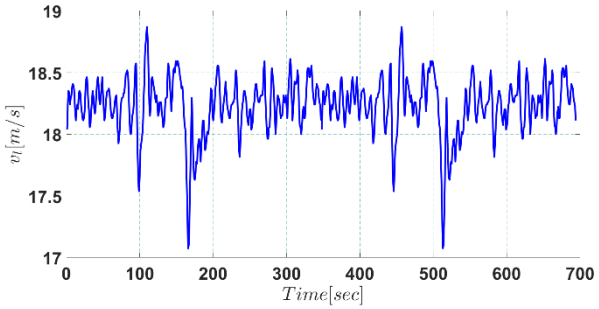

Fig. 3. Speed Profile of Leading Vehicle

The leading vehicle speed profile shown in Fig.3 is obtained by the real-world highway operations of the platform mentioned previously. The original data is 300 seconds and the average speed is around $27m/s(60mph)$. However, the speed is out of the range of the OPD map data collected which is up to around $18m/s(40mph)$. Therefore, the data used in the simulation are scaled down to $40mph$ to fit the OPD map. Furthermore, the cycle was repeated to make sure the time is long enough for ESC to converge. The estimation of acceleration is limited to $(-5m/s^2, 4m/s^2)$ Schafer et al (2020). The relationship of the air drag coefficient with respect to inter-vehicle distance is shown in Fig. 4 according to Davila et al (2013). The profile is the air drag coefficient change of second platoon member of a 4-vehicle platoon. The estimation of acceleration for the leading vehicle is shown in Fig. 6. It can be seen that the overall performance is promising. Some outliers can be observed from the estimations mainly due to the high sensitivity of the observer and the measurement noise which can be neglected.

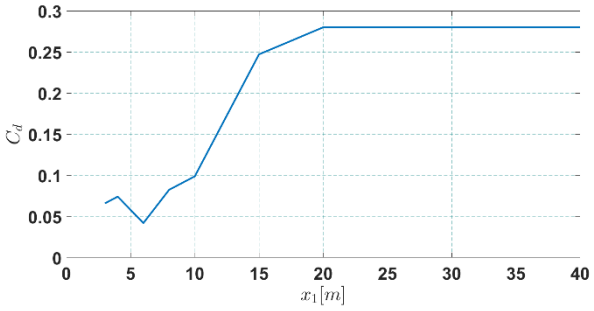

Fig. 4 The Change of Air Drag Coefficient with Inter-Vehicle Distance

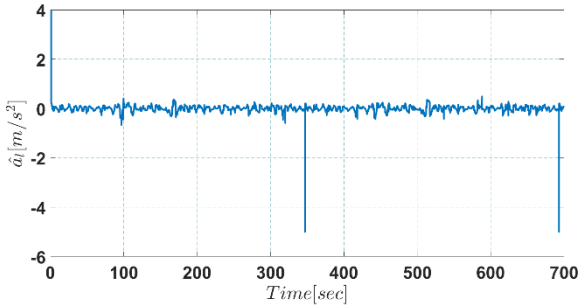

Fig. 5. The Estimated Leading Vehicle Acceleration under ESCWAO

The estimation of aerodynamic drag coefficient for the following vehicle based on the input observer is shown in Fig.6. The design parameter $\gamma = 125$ for the input observer. As observed from this figure, the estimated value is consistent with actual value. The outputs of x_d by standard ESC and ESCWAO are compared in Fig. 7. It is seen from this figure that the ESCWAO algorithm can significantly reduce the steady-state oscillation. The comparison of x_1 among the three controllers is shown in Fig. 8. As it can be seen from Fig. 8, the baseline is able to regulate x_1 to 15 m which is a non-optimal reference value. In comparison, both the standard ESC and ESCWAO scenario can identify the optimal inter-vehicle distance in short periods of time. Compared to the standard ESC, the ESCWAO can significantly reduce steady-state oscillation and thus improve the driving comfort.

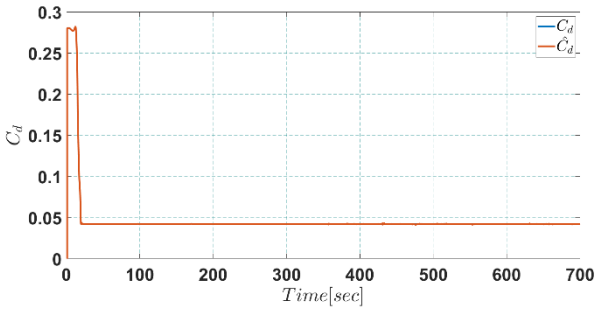

Fig. 6. Estimated Air Drag Coefficient under ESCWAO

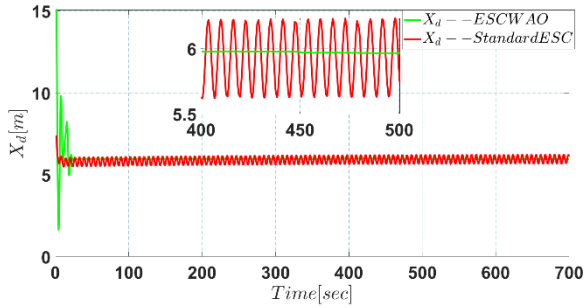

Fig. 7. The Desired Distance Comparison

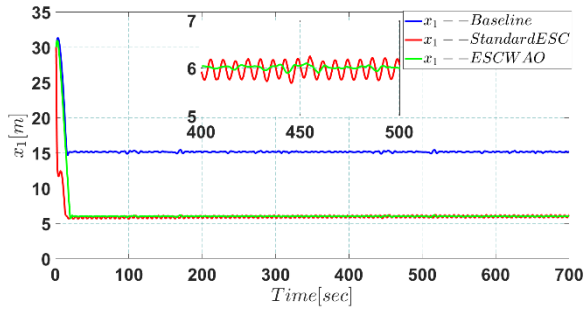

Fig. 8.The Actual Inter-Vehicle Distance Comparison

Fig.9 shows the SOC profiles in that all cases. Compared to the benchmark case, both two ESC based control frameworks result in almost twice longer traveling time using the same amount of energy. Fig. 10 shows the driving range comparison under different controllers. The standard ESC extends the driving range from 128 km to 247 km by 48.14%. The ESCWAO-based control framework extends the driving range to 241km by 46.89%. The driving range improvement of ESCWAO is 2.35 % less than standard ESC. The significant EV range improvement by ESC-based controls can be explained by the following two reasons. First, as explained in the previous subsection, the vehicle speed is around 40 mph at which the electric motor operates at high efficiency and the impact of speed on the energy consumption due to aerodynamic resistance is limited. Secondly, with the proposed ESC-based control framework, the minimum of the air drag coefficient can be achieved, which is only approximately 16.8% of the value in the baseline case. As a result, the energy consumption due to aerodynamic resistance is significantly lower with ESC-based controls than with the baseline control. Another thing that needs to be noticed is that the performance of driving range extension only depends on

the air drag coefficient data used in the simulation. In reality, the improvements may not be magnificent.

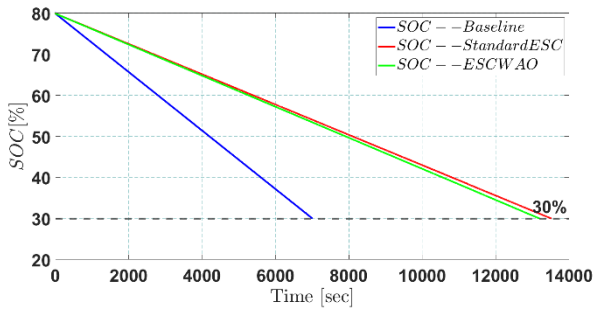

Fig. 9 State of Charge Profiles for Baseline Control and ESC-based Controls

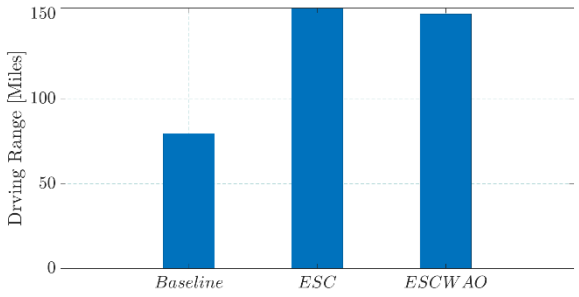

Fig. 9 Comparison of Driving Ranges for Baseline Control and ESC-based Controls

5. CONCLUSIONS AND FUTURE WORK

This paper proposed a hierarchical ESC-based framework to achieve precise inter-vehicle space control and identify the minimum aerodynamic drag coefficient. The simulation results show the capability of the proposed framework in finding and maintaining the inter-vehicle distance that corresponds to the minimum air drag coefficient. In addition, the simulation results demonstrate significant improvement on BEVs' driving range by 46.89%-48.14%. Due to the principle of extremum seeking control, less computational power is required than other optimization methods which makes the real-time application possible. The future work will focus on implementation of the proposed ESC-based control framework on the physical vehicle platform and comprehensive evaluation of its performance in the experiments.

ACKNOWLEDGEMENTS

This work was supported by U.S. Department of Energy under Award No. DE-EE0009223.

REFERENCES

Ariyur, K.B. and Krstic, M., 2003. *Real-time optimization by extremum-seeking control*. John Wiley & Sons.

Bhattacharjee, D. and Subbarao, K., 2021. Extremum seeking control with attenuated steady-state oscillations. *Automatica*, *125*, p.109432.

Chen, P. and Wang, J., 2014, June. Estimation of automotive urea-based selective catalytic reduction systems during low temperature operations. In *2014 American Control Conference* (pp. 1523-1528). IEEE.

Davila, A., Aramburu, E. and Freixas, A., 2013, April. Making the best out of aerodynamics: Platoons. In *SAE 2013 World Congress & Exhibition* (No. 2013-01-0767).

Lamantia, M., Su, Z. and Chen, P., 2021, May. Remaining driving range estimation framework for electric vehicles in platooning applications. In *2021 American Control Conference (ACC)* (pp. 424-429). IEEE.

Namiki, K., Murota, K. and Shoji, M., 2018. *High performance motor and inverter system for a newly developed electric vehicle* (No. 2018-01-0461). SAE Technical Paper.

Ryan, J.J., (2012). *A method of extremum seeking control based on a time varying Kalman filter and its application to formation flight*. University of California, Los Angeles.

Stotsky, A. and Kolmanovsky, I., 2002. Application of input estimation techniques to charge estimation and control in automotive engines. *Control Engineering Practice*, *10*(12), pp.1371-1383.

Schafer, D. and Chen, P., 2020, October. Minimum Safety Distances for Emergency Braking Maneuvers in Car-Following Applications. In *Dynamic Systems and Control Conference* (Vol. 84270, p. V001T02A005). American Society of Mechanical Engineers.

Schafer, D., Lamantia, M. and Chen, P., 2021, May. Modeling and spacing control for an electric vehicle with one-pedal-driving feature. In *2021 American Control Conference (ACC)* (pp. 166-171). IEEE.

Van Boekel, J.J.P., Besselink, I.J.M. and Nijmeijer, H., 2015. Design and realization of a One-Pedal-Driving algorithm for the TU/e Lupo EL. *World Electric Vehicle Journal*, *7*(2), pp.226-237.

Wang, J., Besselink, I.J.M., van Boekel, J.J.P. and Nijmeijer, H., 2015, December. Evaluating the energy efficiency of a one pedal driving algorithm. In *2015 European Battery, Hybrid and Fuel Cell Electric Vehicle Congress (EEVC 2015)*.

Wang, L., Chen, S. and Ma, K., 2016. On stability and application of extremum seeking control without steady-state oscillation. *Automatica*, *68*, pp.18-26.

Yang, S., Su, Z. and Chen, P., 2021, August. Robust Inter-Vehicle Spacing Control for Battery Electric Vehicles with One-Pedal-Driving Feature. In *2021 IEEE Conference on Control Technology and Applications (CCTA)* (pp. 259-264). IEEE.

Zabat, M., Stabile, N., Farascaroli, S. and Browand, F., 1995. The aerodynamic performance of platoons: A final report.